International Food Research Journal 29(5): 1215 - 1225 (October 2022)
Journal homepage: *http://www.ifrj.upm.edu.my*

Emulsification characteristics of soy hull polysaccharides obtained by membrane separation

[1]Wu, X. H., [1]Luo, M. S., [2]Zhao, L., [1]Wang, S. N., [1]Zhu, D. S., [1]*Yang, L. N. and [1]*Liu, H.

[1]*College of Food Science and Technology, Bohai University, Jinzhou, Liaoning, 121013, China*
[2]*College of Food Science and Technology, Jiangnan University, Wuxi, Jiangsu, 214122, China*

Article history

Received:
9 March 2021
Received in revised form:
24 September 2021
Accepted:
1 April 2022

Keywords

emulsification,
membrane separation,
molecular weight,
soy hull polysaccharide

Abstract

Membrane separation technology was used to separate and purify the microwave-assisted oxalic acid extraction of soy hull polysaccharides (MOSP) in order to obtain samples of different molecular weights. The emulsification characteristics of the MOSP were investigated including protein adsorption, polysaccharide adsorption, interfacial tension, emulsion index, and particle size; optical microscopy and Phenom electron microscopy were used to elucidate the emulsion structures. In addition, Fourier transform infrared spectroscopy (FT-IR), atomic force microscopy (AFM), and high-performance gel-filtration chromatography (HPGFC) were used to study the differences in the components and structures of MOSP in different molecular weights. The molecular weight had several important effects on the emulsifying properties of MOSP. The adsorption capacities of the emulsion droplets containing low molecular weight MOSP (L-MOSP), middle molecular weight MOSP (M-MOSP), and high molecular weight MOSP (H-MOSP) were relatively low, and those of H-MOSP were slightly higher than those of L-MOSP. With extended storage time, the particle sizes of the emulsions rich in L-MOSP, M-MOSP, and H-MOSP increased. L-MOSP, M-MOSP, and H-MOSP were mainly composed of furans. The conformation of the molecular chain was spherical. The emulsions formed with H-MOSP were the most stable.

DOI
https://doi.org/10.47836/ifrj.29.5.22

Introduction

Soluble soy polysaccharides (SSPS) are by-product of the production of tofu and soy protein. The main monosaccharide components of SSPS are arabinose, galactose, and galacturonic acid. In addition, SSPS contain small amounts of other monosaccharides such as glucose, fructose, rhamnose, and xylose (Salarbashi *et al.*, 2019). SSPS are compact and spherical molecules, with a rotation radius of approximately 23.5 nm, and an inherent viscosity of 0.33 dL/g at 25°C, comparable with gum Arabic (Wang *et al.*, 2005; Salarbashi *et al.*, 2017). SSPS is water-soluble and has antioxidant, film-forming, and emulsifying properties, and nutritional value. Most polysaccharides form an extended network in the aqueous phase to stabilise an emulsion. Only a few polysaccharides or their derivatives such as gum Arabic, modified starch, and pectin have the ability to adsorb at the oil-water interface (Bouyer *et al.*, 2012). Tran and Rousseau (2013) found that by adding SSPS to an emulsion, the stability of the system could be improved through electrostatic interactions. Zhao *et al.* (2015) investigated the effect of SSPS on the physicochemical properties of lactoferrin-coated orange oil emulsion, and the results showed that the stability of the modified emulsion improved with the adsorption of the polysaccharides. Additionally, much progress has been made toward developing new materials from soy polysaccharides including packaging films, edible films, and environmental protection adhesives (Liu *et al.*, 2020a).

Improving the value of soybean by-products has attracted considerable research attention. Liu *et al.* (2020b) prepared biomass-based carbon materials of sufficient pore size and good electrical conductivity from soybean residue. Fernandes *et al.* (2021) synthesised a biological lubricant using soybean oil by-products as raw materials. Soy hull polysaccharide (SHP) is another SSPS material that has also attracted similar research attention (Li *et al.*,

*Corresponding author.
Email: yangln16@lzu.edu.cn ; liuhe2069@163.com

2022; Lin *et al.*, 2022). In order to conserve resources and improve the value of soy by-products, extracting SHP from the by-products is undoubtedly a good approach. Many researchers have studied methods of extracting SHP. The traditional method of extracting SHP is hot water extraction. This method is simple to perform, and does not require special equipment. However, the yield of the hot water extraction method is low, operating time is lengthy, and considerable energy is consumed (Yi *et al.*, 2020). In comparison, acid and base extraction can improve the yield and purity of the product; but, they are greatly affected by the properties of the extracted material itself. The ultrasonic extraction method can improve the extraction rate, shorten the extraction time, and avoid the influence of high temperature on the extracted components. The microwave extraction method has the advantages of short operating time, strong penetration, high selectivity, high heating efficiency, and ability to destroy the cell wall (Mirzadeh *et al.*, 2020). The methods of extracting SHP are various, and the yield is usually increased by combining multiple extraction methods and auxiliary extraction. Jing *et al.* (2017) optimised ultrasound-assisted extraction of soy polysaccharides by using a single factor experiment and central composite design, and the extracted polysaccharide exhibited high antioxidant activity.

Membrane separation technology is a new and efficient separation technology. Characterised by low energy consumption, high single-stage separation efficiency, simplicity of the process, and lack of environmental pollution, membrane separation technology has been widely used in the chemical, environmental protection, food, medicine, electronics, and other industrial fields (Zhang *et al.*, 2019a). Using membrane separation technology to separate soy polysaccharides is beneficial to the study of the nature of polysaccharides, minimising the limitations of polysaccharides, and expanding the scope of applications of polysaccharides. Tang *et al.* (2020) used a membrane to isolate and purify polysaccharide components from the aqueous extract of *Lentinula edodes*. The results showed that the separated polysaccharide components displayed significant but different immunomodulatory effects, and these components could be good candidates for food and drug development. Xie *et al.* (2019) reported that sodium nitroprusside could be used as an antifouling agent to reduce pollution during polysaccharide membrane separation.

Microwave-assisted oxalic acid extraction of soy hull polysaccharides (MOSP) was classified by membrane separation technology in the present work. The chemical composition, structure, emulsifying activity, and interfacial activity of polysaccharides of different molecular weights were investigated. The emulsification characteristics of MOSP were studied systematically and comprehensively, and the mechanism of emulsification was analysed, which laid a theoretical foundation for MOSP applications.

Materials and methods

Materials

Soy hulls were purchased from the Yu Wang Group of Shan Dong in China (Dezhou, China). Standard monosaccharides were purchased from Pharmacia (NY, USA). DL-A-I gum Arabic (D-galactose, 44%; L-arabinose, 24%; D-glucuronic acid, 14.5%; L-rhamnose, 13%; and 4-o-methyl-O-glucuronic acid, 1.5%) was purchased from Dingli Rubber Co. Ltd. (Taian, China). CA200 soluble soy polysaccharides (moisture: 5.8%; crude protein: 7.8%; crude ash: 7.8%; saccharide composition (%): rhamnose = 5.0, fucose = 3.2, arabinose = 22.6, xylose = 3.7, galactose = 46.1, glucose = 1.2, galacturonic acid = 18.2) were obtained from Buerfuji Technology Co., Ltd. (Beijing, China). All chemicals and solvents were of analytical grade.

MOSP preparation and classification

MOSP were extracted using the methods of Liu *et al.* (2013). Dry soy hull was crushed and passed through a 60-mesh sieve. Then, 1% ethanol solution was added at a ratio of soy hull powder-to-water of 1:10, stirred for 30 min at room temperature, passed through a 200 mesh filter cloth, and dried in an air-dry oven at 65°C. Soy hull residue (50 g) was dispersed in 1 L of water containing 0.6% (wt) oxalic acid (pH 5.43) at 85°C, and maintained at this temperature for 35 min in a microwave extractor (Qihuabo, LD-4, China). The dispersion was then passed through a 200-mesh filter cloth, and centrifuged at 3,500 *g* for 10 min (Backman, Avanti J-25, USA). The supernatant was micro-filtered through 0.2 μm micro-filter and the microfiltrate concentrated using three sequential ultrafiltration membrane separation reactors (Hefei Xinda, XD-G2-D3-4040, China) with molecular weight cut-offs (MWCO) of 50, 10, and 5 kDa. After this, the three filtrates were concentrated in a vacuum rotary

evaporator (Shanghai Yarong, RE-3000A, China), and the pH adjusted to 4.0. Next, concentrated solutions were diluted in ethanol (95%, v/v) at a ratio of 1:2 (v/v) with slow mixing. Precipitates were separated and dried in an air-dry oven at 65°C, and the high molecular weight MOSP (H-MOSP), medium molecular weight MOSP (M-MOSP), and low molecular weight MOSP (L-MOSP) were generated.

Emulsion preparation

An emulsion was produced by homogenising soybean oil (20 wt%), SPI (3 wt%), and MOSPs (L-MOSP, M-MOSP, or H-MOSP) (5 wt%) (Tran and Rousseau, 2013). Solutions were homogenised in a high-speed homogeniser (FJ-200, Specimen Model Factory, Shanghai, China) at 10,000 rpm for 2 min, then homogenised for five times in a high-pressure homogeniser (FB-110S, LiTu Machinery Equipment Engineering Co., Ltd., Shanghai, China) at 35 MPa. After this, emulsions were stored at 4°C for up to 30 d. SPI commercial soluble soy polysaccharide (CA200) and gum Arabic (DL-A-I) (non-SHP) emulsions were prepared identically.

Determining the adsorption capacity of polysaccharides and proteins on emulsion droplets

We centrifuged 1 mL of fresh emulsion at 10,000 *g* for 30 min, after which, the aqueous emulsion phase at the bottom of the tube was pipetted using a syringe, and filtered through a 0.22 μm filter. Protein and polysaccharide concentrations were determined using BCA and phenol-sulphuric acid methods, respectively. The protein or polysaccharide adsorption rate was calculated using Eq. 1:

$$S\ (\%) = \frac{C_a - C_b}{C_a} \times 100\% \quad \text{(Eq. 1)}$$

where, C_a (kg/m^3) and C_b (kg/m^3) = total polysaccharide (or protein) concentrations in initial sample solutions and filtrates, respectively.

Determining interfacial tension in emulsions

SPI/MOSP emulsion interfacial tensions were measured using a video optical contact angle meter (OCA15EC, Dataphysics, Germany) at 25°C. The emulsion density was determined using a densimeter. The emulsion was placed in a syringe, and a fixed volume of sample solution was extruded into the air (Chivero *et al*., 2014).

Determining the emulsion elution index

Emulsion stability procedures were adopted from Karimi and Mohammadifar (2014) with slight modifications. We added 10 mL of fresh emulsion sample to a glass colorimetric tube, and sealed it to prevent evaporation. The sample was stored at room temperature for 30 d, and emulsion stability was regularly determined and expressed using the creaming index (E); Eq. 2:

$$E\ (\%) = \frac{E_a}{E_b} \times 100\% \quad \text{(Eq. 2)}$$

where, E_a and E_b = whey layer height and the total height of the initial emulsion, respectively.

Particle size determination

Emulsion droplet size distribution was measured using a laser particle size distribution meter (BT-9300ST, Baite Instrument Co., Ltd., Dandong, China) according to Xu *et al.* (2017). Results were presented as the surface-weighted mean diameter ($d_{3,2}$) and size distribution. The parameters were: scattering angle = 90°, laser wavelength = 633 nm, temperature = 25°C, particle refractive index = 1.596, particle absorption index = 0.001, dispersant = water, and dispersant refractive index = 1.333.

Microscopic analysis

Emulsion microstructures were observed using an upright microscope (Nikon 80i, Japan) and a Phenom Pro Electron Microscope (Phenom-World, Netherlands).

Determining the relative molecular weight of MOSP components

We determined the relative molecular weight of MOSP components using HPGFC (1525, Waters, USA) equipped with a 2414 differential refractive detector and Empower 3 workstation. MOSPs were dissolved in 0.1 mol/L $NaNO_3$ ultrapure water. The mass concentration was 10 mg/mL. After filtration using a microporous filter membrane, gel permeation filtration chromatography was performed. Chromatographic conditions: injection volume = 20 μL, ultrahydrogel™ linear column (300 × 7.8 mm; Waters, USA); velocity = 0.9 mL/min; and column temperature = 45°C. Molecular weight standards for the correction curve was determined using DextranT series. The average molecular weight (M_W) of DextranT series was 1.338×10^5, 4.11×10^4, 2.5×10^3, and 1×10^3, respectively.

Determining basic MOSP components

The total sugar content was determined using a phenol-sulphuric acid method (Dubois *et al.*, 1956). The moisture was determined by direct drying. The proteins were measured using the Kjeldahl method (Kong *et al.*, 2015; Malgorzata *et al.*, 2019).

MOSP monosaccharide composition

We dissolved 5 mg of MOSP in 4 mol/L trifluoroacetic acid (TFA) solution, and placed it in an oven at 110°C for 6 h, with methanol added repeatedly. Then, it was blown dry in a nitrogen blower, and lastly deionised water was used to fix the volume to 25 mL. To 0.1 μL of hydrolysed samples and monosaccharides, alditol acetate was added, and the solution was injected into an ion chromatograph (ICS-5000, Dionex, USA) equipped with a Carbopac PA20 column (150 × 3 mm) and a flame ionisation detector. The column temperature was programmed to increase from 130 to 170°C at 5°C/min, and then to 250°C at 2°C/min. The injection temperature = 280°C, detector temperature = 300°C, and the N_2 carrier gas flow rate was 0.5 mL/min (Zhang *et al.*, 2020).

Zeta-potential measurements

A laser particle size distributor (NANO ZS90, Malvern Instruments Ltd., UK) was used to determine the zeta potential of emulsions at 20°C (Anvari *et al.*, 2016). We 10-fold diluted 1 mL of emulsion in water into the sample pool for determination.

Fourier transform infrared spectroscopy (FT-IR) MOSP analysis

Briefly, 1 mg samples that was removed from free water was mixed with KBr and ground by pressing to generate a pressing sheet. Before testing, a blank correction was conducted to remove interference factors (CO_2 and air humidity) and scanned for more than 32 times. FT-IR spectra were recorded from 400 to 4000 cm^{-1} in a Scimitar 2000 Near FT-IR Spectrometer (Agilent Technologies, Santa Clara, USA) (Wei *et al.*, 2016).

Atomic force microscopy (AFM) MOSP analysis

MOSP were examined using an XE-70 AFM instrument (Park Systems Co., Seoul, Korea). We dissolved 20 mg of MOSP in 100 mL of ddH_2O, stirred the solution for 12 h at room temperature, and filtered it through a 0.22 μm filter membrane. Samples were diluted to 5 mg/L in water, and heated at 85°C for 10 min, then filtered through a 0.22 μm filter membrane. Then, 5 μL of the MOSP solution (5 mg/L) was dropped directly onto the surface of a mica carrier, and dried at 70°C under ambient pressure. A tapping mode was adopted, and the scanning frequency was 1.00l Hz. The needle tip was Si, and images were collected in constant force mode.

Statistical analysis

All measurements were performed three times. Test data were represented by the mean ± standard deviation (SD). Origin 19.1 software was used for plotting graphs, and SPSS 19.0 software (IBM Corp, Armonk, NY, USA) was used for ANOVA. Results were considered statistically significant at $p < 0.05$.

Results and discussion

Interfacial tension, surface adsorption, and creaming index of the emulsions

The data in Figure 1(a) show that the adsorption capacities of protein on emulsions containing L-MOSP, M-MOSP, and H-MOSP were 33.76, 39.45, and 46.33%, respectively, and those of protein on emulsions containing CA200 and DL-A-I were 30.29 and 28.25%, respectively. Due to its amphiphilic structure, the protein could form a viscoelastic protective film at the oil droplet interface, which provides long-term stability for the emulsion through spatial and electrostatic stabilisation mechanisms (Gunning *et al.*, 2004). With the increase in relative molecular weight, the amount of protein adsorption gradually increased, possibly because polysaccharides with greater molecular weights have more negative charges, thus leading to more interactions with the protein and adsorption to the oil-water interface (Shao *et al.*, 2020). Data in Figure 1(b) show that the adsorption percentages of L-MOSP, M-MOSP, and H-MOSP on the droplet surface were 48.37, 54.09, and 56.63%, respectively, and the adsorption capacities of CA200 and DL-A-I on the emulsion surface were 18.93 and 27.90%, respectively. The adsorption capacity of the high molecular weight polysaccharides was slightly higher than that of the low molecular weight polysaccharides, probably because of the strong interfacial activity of the high molecular weight polysaccharides; so, there were more polysaccharide molecules absorbed at the oil-water interface. The high molecular weight polysaccharides had higher protein and polysaccharide adsorption capacities on

the emulsion surface which increased the interaction between polysaccharide and protein, and that interaction has an important influence on the adsorption of protein on the interfacial layer (Xiong *et al.*, 2016).

Data in Figure 1(c) show that interfacial tensions of L-MOSP, M-MOSP, and H-MOSP emulsions were relatively high at 47.32, 46.89, and 46.94 mN/m, respectively. With increasing SHP molecular weight, the tension gradually decreased. Additionally, these tensions were lower than the DL-A-I emulsion (50.25 mN/m), and higher than the CA200 emulsion (46.29 mN/m). In terms of SHP morphology, H-MOSP comprised a thick sugar chain, thus enabling more closely packaged proteins and polysaccharides, which in turn, generating good molecular interactions which were rapidly adsorbed onto the gas-water interface to reduce interfacial tension (Ding *et al.*, 2017). Hence, the interfacial activity of SHP generated by H-MOSP was higher than DL-A-I.

The data in Figure 1(d) show that M-MOSP and H-MOSP displayed good storage stability as no obvious emulsion evolution was observed after four weeks of storage at room temperature. In the control group, CA200, and DL-A-I, the phenomenon of creaming appeared at 5 d. Creaming of SNOL was observed at 25 d (Creaming index increased from 3.41 to 5.23%). When proteins and charged polysaccharides are introduced at the same time, the diffusion, adsorption, and recombination of the two biopolymers are affected to varying degrees due to the electrostatic interaction between them (Dickinson, 2008). After the separation and purification of M-MOSP and H-MOSP by membranes, the amounts of proteins and polysaccharides adsorbed were higher. Through electrostatic interactions, polysaccharide and protein molecules adhere to each other to enhance the interfacial activity, thus improving the stability of the emulsion which was consistent with the amount of adsorption noted on the emulsion surface. Other reports have also shown that gum Arabic stabilises emulsions through electrostatic repulsion and spatial interactions (Hu *et al.*, 2019).

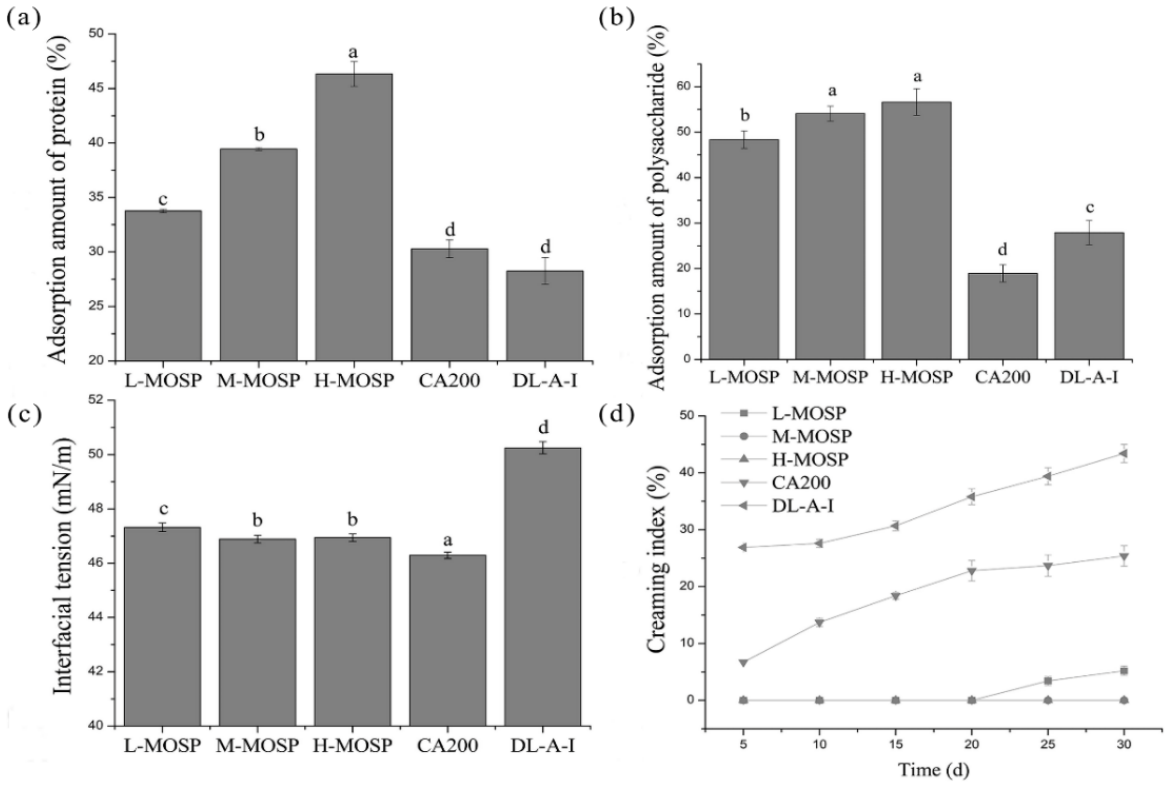

Figure 1. Interfacial tension, surface adsorption, and emulsion evolution index of emulsion. Adsorption amount of protein in the emulsion droplets **(a)**; adsorption amount of polysaccharide in the emulsion droplets **(b)**; interfacial tension of the emulsion **(c)**; and Creaming index of the emulsion **(d)**. Different lowercase letters indicate significant difference ($p < 0.05$).

Particle size distribution of the emulsions

The particle size distributions of emulsions are shown in Figure 2. The droplet sizes of L-MOSP, M-MOSP, and H-MOSP were smaller than CA200 and DL-A-I. Specifically, particle-size distributions of L-MOSP, M-MOSP, and H-MOSP emulsions were small and uniform, thus suggesting good stability. This might have been due to high molecular weights, longer hydrophobic groups, negatively charged surfaces, stronger electrostatic effects, and spatial steric hindrance (Nakamura *et al.*, 2006). With increased time, the particle size distribution range of L-MOSP, M-MOSP, and H-MOSP emulsions substantially increased, and particle size distribution curves shifted to larger sizes, which might have led to emulsion stratification and oil-water separation.

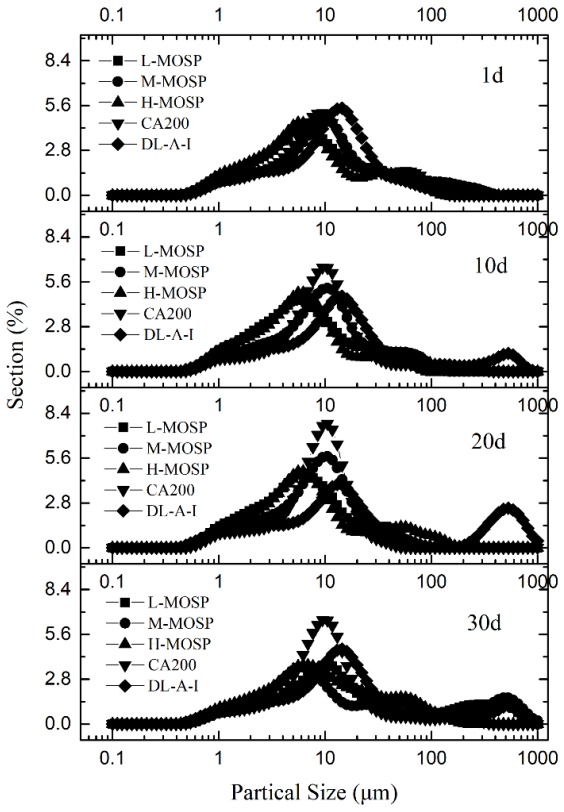

Figure 2. Particle size changes of five different emulsions on days 1, 10, 20, and 30.

Emulsion structures

As shown in Figure 3(a), the optical microscopy images of the emulsions indicate that the oil droplets containing M-MOSP and H-MOSP were similar in size and distributed evenly with no obvious aggregation. The oil droplets in the emulsion containing L-MOSP tended to aggregate. When CA200 and DL-A-I were added to the emulsion, the sizes of oil droplets were not uniform, and there was obvious aggregation.

In Figure 3(b) the electron microscopy images of the emulsions show that the emulsions with M-MOSP, H-MOSP, and CA200 added formed a dense network structure with uniform distributions of oil droplets. However, the addition of L-MOSP to the emulsion caused the formation of a weak network structure, and the oil droplets were unevenly distributed with large pores. The oil droplets in the emulsion with added DL-A-I aggregated to form lumps. This might have been due to the absolute value of the zeta potential of the L-MOSP emulsion that was small, and the contents of interfacial proteins and polysaccharides adsorbed that were also small, thus leading to poor relative stability. The interactions between M-MOSP and H-MOSP and soy protein improved the surface roughness of soy polysaccharide as well as its interfacial adsorption property and the emulsion stability (Zhang *et al.*, 2019b). The interfacial adsorption of DL-A-I was poor, and the emulsion layers agglomerated with each other.

Component analysis and zeta potential of the MOSP

As shown in Table 1, the weight average molecular weight (Mw) and number average molecular weight (Mn) of the H-MOSP were 251.70 and 31.83 kDa, respectively, which were higher than those of M-MOSP (157.61 and 27.46 kDa) and L-MOSP (137.56 and 23.57 kDa). Furthermore, the polydispersity indices (PDI = Mw/Mn, 3.41 - 5.90) indicated that L-MOSP and M-MOSP formed polydisperse aggregates (Salarbashi *et al.*, 2018). The PDI value of H-MOSP was the largest, while the PDI value of M-MOSP was the smallest, thus indicating that M-MOSP exhibited better uniformity than L-MOSP and H-MOSP. L-MOSP, M-MOSP, and H-MOSP were mainly composed of mannose, galactose, and arabinose. The mannose, galactose, and arabinose contents of L-MOSP were 52.957, 15.573, and 28.011%. Those of M-MOSP were 49.674, 15.307, and 31.152%, and those of H-MOSP were 51.134, 14.723, and 30.875%, respectively. These results showed that mannose, galactose, and arabinose were the main MSOP components. MOSP displayed a monosaccharide composition distinct to SSPS in previous research (Salarbashi *et al.*, 2019). These

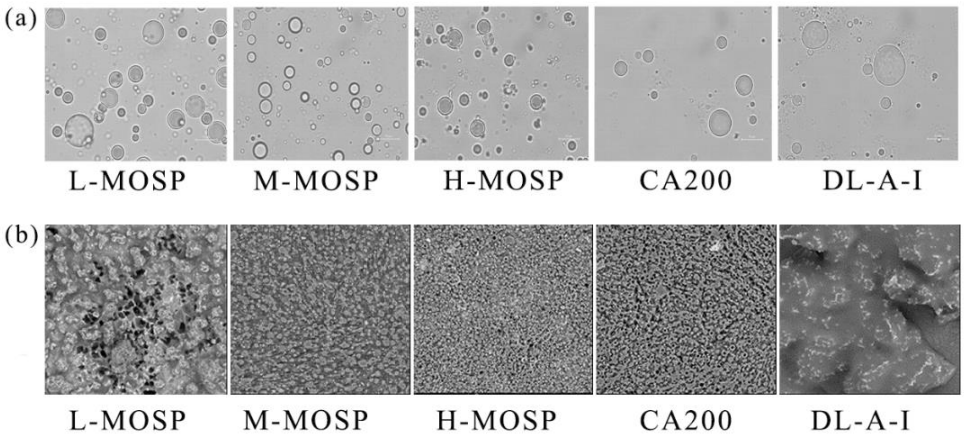

Figure 3. Microstructure of emulsion. Light microscope of emulsion **(a)**; and Phenom electron microscope of emulsion **(b)**.

Table 1. Chemical composition, zeta potential, and molecular weight distribution of MOSP.

Sample	L-MOSP	M-MOSP	H-MOSP
Moisture content (%)	12.74 ± 0.06[a]	10.56 ± 0.09[c]	11.34 ± 0.08[b]
Total sugar content (%)	65.79 ± 0.06[a]	67.31 ± 0.05[a]	68.12 ± 0.05[a]
Protein content (%)	3.06 ± 0.05[a]	3.39 ± 0.01[a]	3.78 ± 0.01[a]
Zeta potential (mV)	-9.72 ± 0.49[a]	-11.10 ± 0.61[a]	-11.80 ± 0.68[a]
Conductivity (S/m)	1.407 ± 0.075[a]	1.605 ± 0.069[a]	1.730 ± 0.044[a]
Rhamnose (%)	1.252	1.605	1.336
Arabinose (%)	28.011	31.152	30.875
Galactose (%)	15.573	15.307	14.723
Glucose (%)	1.327	1.311	1.024
Mannose (%)	52.957	49.674	51.134
Galacturonic acid (%)	0.880	0.951	0.909
Mn	23572	27455	31831
Mw	137562	157612	251701
Mw/Mn	5.836	5.741	7.907

Different lowercase superscripts indicate significant difference ($p < 0.05$).

results indicated that the soy polysaccharides extracted from different sources and by different methods contained different monosaccharides, and membrane separation did not affect the monosaccharide composition in MOSP. The protein contents of L-MOSP, M-MOSP, and H-MOSP were relatively low at 3.06, 3.39, and 3.78%, respectively.

The attractions and repulsions between colloidal particles have important effects on the stability and physical and chemical properties of colloids (Dai *et al.*, 2017). The surfaces of the emulsions formed by L-MOSP, M-MOSP, and H-MOSP were negatively charged, and the absolute values of the zeta potentials and conductivities of the emulsions increased with increases in the relative molecular mass. The zeta potentials of solutions higher than +30 mV or lower than -30 mV is considered stable, since the repulsive forces between particles are maintained during dispersion (Wei *et al.*, 2016). The results (Table 1) show that the three emulsions had low zeta potentials and poor stabilities. It is possible that the presence of more neutral sugars reduced the conductivities. This indicates that the interactions between the anionic polysaccharides and proteins were mainly electrostatic attractions, which is the same conclusion as that proposed by Liu *et al.* (2016).

Fourier transform infrared spectroscopy (FT-IR) and atomic force microscopy (AFM) of the MOSP

FT-IR L-MOSP, M-MOSP, and H-MOSP spectra are shown in Figure 4. Fraction spectra were similar to each other. The strong and wide absorption peak near 3500 - 3400 cm^{-1} was considered a tensile vibration of -OH, while the weak absorption peak near 2923 cm^{-1} was due to the methyl C-H group in the sugar ring (Li *et al.*, 2017). These peaks were characteristic of polysaccharide groups. The characteristic absorption peak near 1735 cm^{-1} was related to the stretching vibration of a C = O bond, and the absorption peak at 1620 cm^{-1} was the bending vibration absorption of an N-H bond. These peaks could have been caused by the presence of uronic acid. In addition, the 1147 cm^{-1} peak was associated with the vibration of C-O-C or C-O-H groups (Li *et al.*, 2015), thus suggesting that all MOSP components contained pyranoid rings. The peak at 769 cm^{-1} indicated the stretching vibration of a symmetric pyran ring (Wang *et al.*, 2005). These results suggested that membrane separation had little effect on SHP structure (Yang *et al.*, 2019).

AFM images of L-MOSP, M-MOSP, and H-MOSP are also shown in Figure 4. M-MOSP was dominated by spherical molecular chains which were between 10.5 and 89.4 nm in diameter. H-MOSP was also dominated by spherical molecular chains with diameters ranging from 15.4 to 257.5 nm. M-MOSP and H-MOSP emulsions were added to form a dense network structure with a uniform oil droplet size distribution. L-MOSP was aggregated, with a diameter range of 11.01 - 25.4 nm. The L-MOSP emulsion formed a weak network structure with an uneven oil droplet size distribution and large pores. This might have been due to the absolute zeta potential value of the L-MOSP emulsion that was small, and the level of interfacial adsorbed proteins and polysaccharides that were also small, thus resulting in relatively poor stability. When DL-A-I was added, the droplets gathered and displayed poor stability.

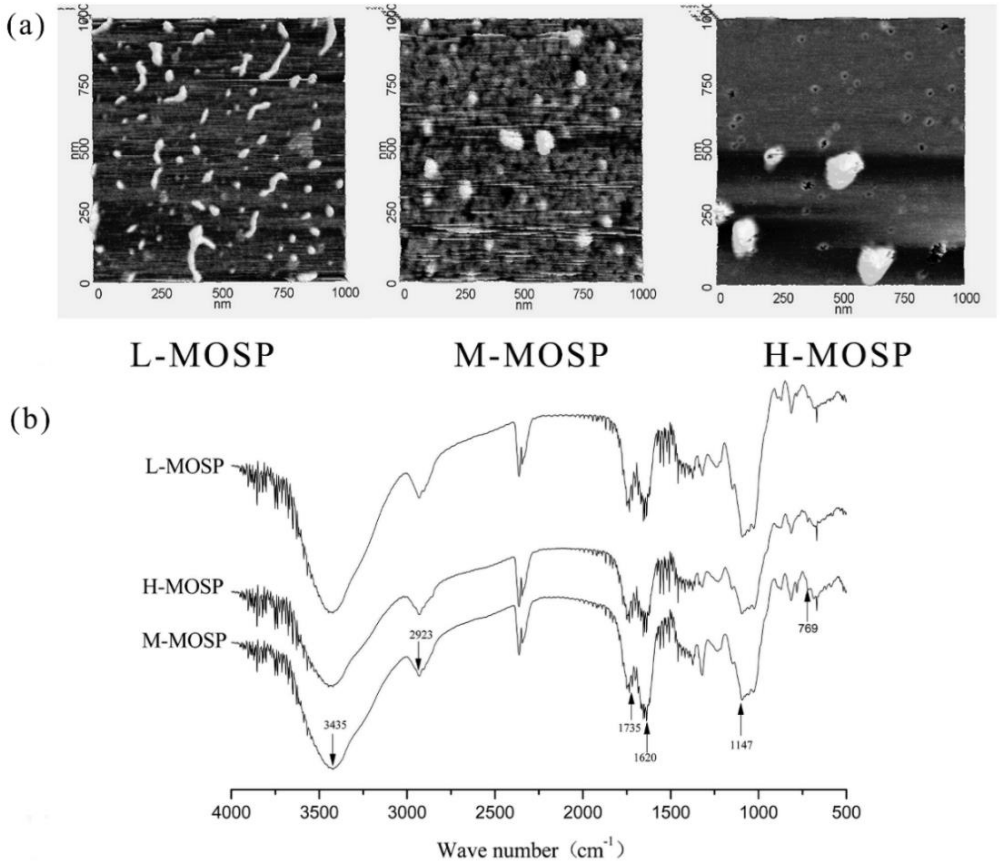

Figure 4. AFM and FT-IR of MOSP. Comparison of AFM images of MOSP **(a)**; and FT-IR spectra of MOSP fractions from 500 to 4000 cm^{-1} **(b)**.

Conclusion

SHPs of different molecular weights were obtained by membrane separation. The polysaccharides had better emulsification stability than commercial CA200 and DL-A-I, of which H-MOSP displayed the most outstanding emulsification stability. This emulsion had a higher viscosity, uniform particle size distribution, small particle size, small interfacial tension, and a high absolute zeta potential value. The emulsion was also stored for 30 d without obvious emulsion evolution. Also, it formed a dense network structure. Molecular weight had an important effect on the emulsifying stability of soy hull polysaccharides; they were better due to their higher molecular weight, longer hydrophobic groups, more negative surface charges, stronger electrostatic effects, and steric hindrance, thereby stabilising the emulsion. Polysaccharides separated by membranes had better specificity and efficiency; however, the specific ability of each component must be explored in future work.

Separating polysaccharides using membrane separation technology was highly efficient, and could expand the application of polysaccharides to foods and other fields, especially the food emulsification sector. Importantly, we provided a theoretical basis for the development of soy hull polysaccharide food emulsifiers which could alleviate the serious shortage of natural plant polysaccharide emulsifiers. Also, our research can be used for the rational development and increased use of rich soybean resources.

Acknowledgement

The present work was financially supported by the National Natural Science Foundation of China (grant no.: 31972031).

References

Anvari, M., Tabarsa, M., Cao, R., You, S., Joyner, H. S., Behnam, S. and Rezaei, M. 2016. Compositional characterization and rheological properties of an anionic gum from *Alyssum homolocarpum* seeds. Food Hydrocolloids 52: 766-773.

Bouyer, E., Mekhloufi, G., Rosilio, V., Grossiord, J.-L. and Agnely, F. 2012. Proteins, polysaccharides, and their complexes used as stabilizers for emulsions: Alternatives to synthetic surfactants in the pharmaceutical field? International Journal of Pharmaceutics 436(1-2): 359-378.

Chivero, P., Gohtani, S., Yoshii, H. and Nakamura, A. 2014. Physical properties of oil-in-water emulsions as a function of oil and soy soluble polysaccharide types. Food Hydrocolloids 39: 34-40.

Dai, S., Jiang, F., Shah, N. P. and Corke, H. 2017. Stability and phase behavior of konjac glucomannan-milk systems. Food Hydrocolloids 73: 30-40.

Dickinson, E. 2008. Interfacial structure and stability of food emulsions as affected by protein-polysaccharide interactions. Soft Matter 4(5): 932-942.

Ding, J., Ma, W. J., Bi, S., Qi, B. K., Wang, Z. J., Sui, X. N. and Jiang, L. Z. 2017. Effect of ultra-high pressure modified soy protein and soluble polysaccharide complex on emulsion formation and stability. Food Science 38: 104-109.

Dubois, M., Gilles, K. A., Hamilton, J. K., Rebers P. A. and Smith F. 1956. Colorimetric method for determination of sugars and related substances. Analytical Chemistry 28: 350-356.

Fernandes, K. V., Cavalcanti, E. D. C., Cipolatti, E. P., Aguieiras, E. C. G., Pinto, M. C. C., Tavares, F. A., ... and Freire, D. M. G. 2021. Enzymatic synthesis of biolubricants from by-product of soybean oil processing catalyzed by different biocatalysts of *Candida rugosa* lipase. Catalysis Today 362: 122-129.

Gunning, P. A., Mackie, A. R., Gunning, A. P., Wilde, P. J., Woodward, N. C. and Morris, V. J. 2004. The effect of surfactant type on protein displacement from the air-water interface. Food Hydrocolloids 18(3): 509-515.

Hu, B., Han, L., Kong, H., Nishinari, K., Phillips, G. O., Yang, J. and Fang, Y. 2019. Preparation and emulsifying properties of trace elements fortified gum Arabic. Food Hydrocolloids 88: 43-49.

Jing, C. L., Yuan, Y., Tang, Q., Zou, P., Li, Y. and Zhang, C. 2017. Extraction optimization, preliminary characterization and antioxidant activities of polysaccharides from *Glycine soja*. International Journal of Biological Macromolecules 103: 1207-1216.

Karimi, N. and Mohammadifar, M. A. 2014. Role of water soluble and water swellable fractions of gum tragacanth on stability and characteristic of model oil in water emulsion. Food Hydrocolloids 37: 124-133.

Kong, L., Yu, L., Feng, T., Yin, X. J., Liu, T. J. and Dong L. 2015. Physicochemical characterization of the polysaccharide from *Bletilla striata*: Effect of drying method. Carbohydrate Polymers 125: 1-8.

Li, J. E., Wang, W. J., Zheng, G. D. and Li, L. Y. 2017. Physicochemical properties and antioxidant activities of polysaccharides from *Gynura procumbens* leaves by fractional precipitation. International Journal of Biological Macromolecules 95: 719-724.

Li, L., Zhao, Y. F., Li, J. Q., Ban, L. Z., Yang, L. N., Wang, S. N., … and Liu, H. 2022. The adhesion of the gut microbiota to insoluble dietary fiber from soy hulls promoted the proliferation of probiotics *in vitro*. LWT - Food Science and Technology 153: 112560.

Li, S. C., Yang, X. M., Ma, H. L., Yan, J. K. and Guo, D. Z. 2015. Purification, characterization and antitumor activity of polysaccharides extracted from *Phellinus igniarius* mycelia. Carbohydrate Polymers 133: 24-30.

Lin, Q., Yang, L. N., Han, L., Wang, Z. Y., Luo, M. S., Zhu, D. S., … and Feng, Y. 2022. Effects of soy hull polysaccharide on dyslipidemia and pathoglycemia in rats induced by a high-fat-high-sucrose diet. Food Science and Human Wellness 11: 49-57.

Liu, C., Huang, J., Zheng, X., Liu, S., Lu, K., Tang, K. and Liu, J. 2020a. Heat sealable soluble soybean polysaccharide/gelatin blend edible films for food packaging applications. Food Packaging and Shelf Life 24: 100485.

Liu, H., Li, Q., Zhu, D., Li, J., Liu, J., Geng, P. and He, Y. 2013. Effects of sucrose and urea on soy hull pectic polysaccharide gel induced by D-glucono-1,5-lactone. Carbohydrate Polymers 98(1): 542-545.

Liu, H., Xie, Y., Wei, P., Wang, W., Chen, H., Geng, C. and Qiang, Y. 2020b. Interface optimization of hole-conductor free perovskite solar cells using porous carbon materials derived from biomass soybean dregs as a cathode. Journal of Alloys and Compounds 842: 1-9.

Liu, L. Y., Zhao, Q. Z., Zhou, S. M. and Zhao, M. M. 2016. Modulating interfacial dilatational properties by electrostatic sodium caseinate and carboxymethylcellulose interactions. Food Hydrocolloids 56: 303-310.

Malgorzata, B., Monika, B., Pawel, A. and Piotr, B. H. 2019. Adherence of Group B Streptococci to human rectal and vaginal epithelial cell lines in relation to capsular polysaccharides as well as alpha-like protein genes - pilot study. Polish Journal of Microbiology 62: 85-90.

Mirzadeh, M., Arianejad, M. R. and Khedmat, L. 2020. Antioxidant, antiradical, and antimicrobial activities of polysaccharides obtained by microwave-assisted extraction method: A review. Carbohydrate Polymers 229: 115421.

Nakamura, A., Yoshida, R., Maeda, H. and Corredig, M. 2006. Soy soluble polysaccharide stabilization at oil-water interfaces. Food Hydrocolloids 20(23): 277-283.

Salarbashi, D., Bazeli, J. and Tafaghodi, M. 2019. Environment-friendly green composites based on soluble soybean polysaccharide: A review. International Journal of Biological Macromolecules 122: 216-223.

Salarbashi, D., Noghabi, M. S., Bazzaz, B. S. F., Shahabi-Ghahfarrokhi, I., Jafari, B. and Ahmadi, R. 2017. Eco-friendly soluble soybean polysaccharide/nanoclay Na^+ bionanocomposite: Properties and characterization. Carbohydrate Polymers 169: 524-532.

Salarbashi, D., Tafaghodi, M., Bazzaz, B. S. F. and Jafari, B. 2018. Characterization of soluble soybean (SSPS) polysaccharide and development of eco-friendly SSPS/TiO_2 nanoparticle bionanocomposites. International Journal of Biological Macromolecules 112: 852-861.

Shao, P., Feng, J., Sun, P., Xiang, N., Lu, B. and Qiu, D. 2020. Recent advances in improving stability of food emulsion by plant polysaccharides. Food Research International 137: 109376

Tang, W., Liu, C. C., Liu, J. J., Hu, L. Y., Huang, Y. S., Yuan, L., ... and Nie, S. P. 2020. Purification of polysaccharide from *Lentinus edodes* water extract by membrane separation and its chemical composition and structure characterization. Food Hydrocolloids 105: 105851.

Tran, T. and Rousseau, D. 2013. Stabilization of acidic soy protein-based dispersions and emulsions by soy soluble polysaccharides. Food Hydrocolloids 30(1): 382-392.

Wang, Q., Huang, X. Q., Nakamura, A., Burchard, W. and Hallett, F. R. 2005. Molecular characterisation of soybean polysaccharides: An approach by size exclusion chromatography, dynamic and static light scattering methods. Carbohydrate Research 340(17): 2637-2644.

Wei, C. Y., Li, W. Q., Shao, S. S., He, L., Cheng, J., Han, S. and Liu, Y. 2016. Structure and chain conformation of a neutral intracellular heteropolysaccharide from mycelium of *Paecilomyces cicadae*. Carbohydrate Polymers 136: 728-737.

Xie, Z., Skillman, L., Nagaraj, V., Li, D. and Ho, G. 2019. Experimental investigation into the use of sodium nitroprusside for controlling polysaccharide fouling in membrane separation. Journal of Water Process Engineering 27: 171-176.

Xiong, W., Ren, C., Jin, W., Tian, J., Wang, Y., Shah, B. R., ... and Li, B. 2016. Ovalbumin-chitosan complex coacervation: Phase behavior, thermodynamic and rheological properties. Food Hydrocolloids 61: 895-902.

Xu, X., Liu, W., Luo, L., Liu, C. and McClements, D. J. 2017. Influence of anionic polysaccharides on the physical and oxidative stability of hydrolyzed rice glutelin emulsions: Impact of polysaccharide type and pH. Food Hydrocolloids 72: 185-194.

Yang, L. N., Zhang, H. Y., Zhao, Y. F., Huang, J. H., Zhao, L., Lin, Q. and Liu, H. 2019. Chemical compositions and prebiotic activity of soy hull polysaccharides *in vitro*. Food Science and Technology Research 25: 843-851.

Yi, Y., Xu, W., Wang, H. X., Huang, F. and Wang, L. M. 2020. Natural polysaccharides experience physiochemical and functional changes during preparation: A review. Carbohydrate Polymers 234: 115896.

Zhang, R. Y., Huang, Y., Sun, C. B., Liang, X. Z., Bentian, X. and Wang, Z. J. 2019a. Study on ultrasonic techniques for enhancing the separation process of membrane. Ultrasonics Sonochemistry 55: 341-347.

Zhang, X. Z., Liu, Y. L., Wang, Y. X., Luo, X. G., Li, Y., Li, B., ... and Liu, S. L. 2019b. Surface modification of cellulose nanofibrils with protein nanoparticles for enhancing the stabilization of O/W pickering emulsions. Food Hydrocolloids 97: 105180.

Zhang, Y., Zeng, Y., Cui, Y. S., Liu, H. M., Dong, C. X. and Sun, Y. X. 2020. Structural characterization, antioxidant and immunomodulatory activities of a neutral polysaccharide from *Cordyceps militaris* cultivated on hull-less barley. Carbohydrate Polymers 235: 115969.

Zhao, J. J., Wei, T., Wei, Z. H., Yuan, F. and Gao, Y. X. 2015. Influence of soybean soluble polysaccharides and beet pectin on the physicochemical properties of lactoferrin-coated orange oil emulsion. Food Hydrocolloids 44: 443-452.